JOC Article
pubs.acs.org/joc

Asymmetry in the *N*-Inversion of Heteroarene Imines: Pyrimidin-4(3*H*)-Imine, Pyridin-2(1*H*)-Imine, and 1*H*-Purine-6(9*H*)-Imine

Rainer Glaser,* Jian Yin, and Stephanie Miller

Department of Chemistry, University of Missouri, Columbia, Missouri 65211

glaserr@missouri.edu

Received November 4, 2009

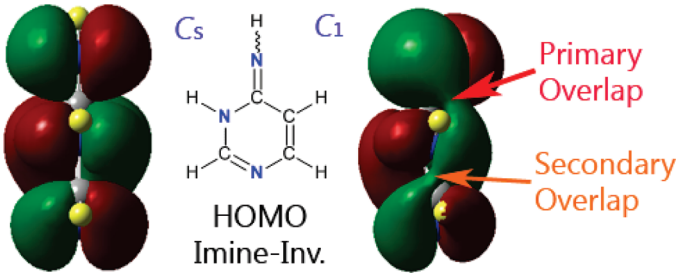

The uncatalyzed, thermal *N*-inversion reactions were studied of pyrimidin-4(3*H*)-imine (**PMI**), pyridin-2(1*H*)-imine (**PYI**), and 1*H*-purine-6(9*H*)-imine (**PUI**). Relevant regions of the potential energy surfaces were explored with second-order Møller−Plesset perturbation theory (MP2(full)/6-31G(d)) and with coupled cluster theory (CCSD/6-31G(d), CCSD/6-31+G(d)). The thermochemistry of stationary structures was evaluated at the MP2 level and their energies also were computed at the levels CCSD(T)/6-311+G(d,p) and CCSD(T)/6-311+G(2df,2p) and with structures optimized at lower CCSD levels. The best estimates for the (*E*)-preference free enthalpies ΔG_{298}(*Z* vs. *E*) are 2.6 (**PMI**), 2.3 (**PYI**), and 6.0 (**PUI**) kcal/mol and for the free enthalpies of activation $\Delta G_{298}(Z \rightarrow E)$ they are 21.6 (**PMI**), 21.1 (**PYI**) and 19.7 (**PUI**) kcal/mol. Nonplanar *N*-inversion transition state (ITS) structures occur along enantiomeric reaction paths and stationary structures for in-plane N-inversion correspond to second-order saddle points (SOSP) on the potential energy surface. The deformation energy $\Delta E_{def} = E(\text{SOSP}) - E(\text{ITS})$ is less than 0.5 kcal/mol for **PMI** and **PUI**, but it is as high as $\Delta E_{def} \approx 2$ kcal/mol for **PYI**. The detailed study of structures and electronic structures along the entire *N*-inversion path of the isomerization (*Z*)-**PMI** ⇄ (*E*)-**PMI** revealed a remarkable stabilization due to asymmetry in the ascent region from the (*E*)-isomer to ITS. Structures in this region of the potential energy surface allow best for additional bonding overlaps in the HOMO, and this amidine effect predicts lower *N*-inversion barriers in analogous imines with (*Z*)-preference energies. The discussion of the halogen-bonded aggregate **PMI**·$ClCH_3$ exemplifies that the asymmetry in *N*-inversion paths is retained and perhaps even enhanced in chlorinated solvents of low polarity.

Introduction

Adenine **1** formally is a pentamer of HCN and HCN pentamerization indeed leads to the formation of adenine. We have been interested in the mechanisms for the formation of the pyrimidine ring from the monocyclic HCN-pentamer, substrate **S2**, and tandem pericyclic reaction offers one path (Scheme 1).[1] The sequence of hydrogen transfer by way of [1,7]-sigmatropic rearrangement of an amino-H to the nitrile-N and subsequent electrocyclization leads to the (*Z*)-imino form of 9*H*-adenine **2** (1*H*-purine-6(9*H*)-imine, **PUI**), and the isomerization (*Z*)-**2** to (*E*)-**2** prepares the stage for tautomerization of **2** to **1**. The analogous reaction sequence converts the dieneyne-type models **SPMI** and **SPYI** to pyrimidine and pyridine derivatives, respectively; **SPMI** to 4-aminopyrimidine **APM** via pyrimidin-4(3*H*)-imine **PMI** and **SPYI** to 4-aminopyridine **APY** via pyridine-2(1*H*)-imine **PMI**.

(1) Glaser, R.; Hodgen, B.; Farrelly, D.; McKee, E. Adenine Synthesis in Interstellar Space: Mechanisms of Prebiotic Pyrimidine Ring-Formation in Monocyclic HCN-Pentamers. In *Astrobiology* **2007**, *7*, 455–470.

Published on Web 01/28/2010 DOI: 10.1021/jo902358c

SCHEME 1. **(*Z*)/(*E*)-Isomerization of 1*H*-Purine-6(9*H*)-imine, Pyrimidin-4(3*H*)-imine, and Pyridin-2(1*H*)-imine in Context

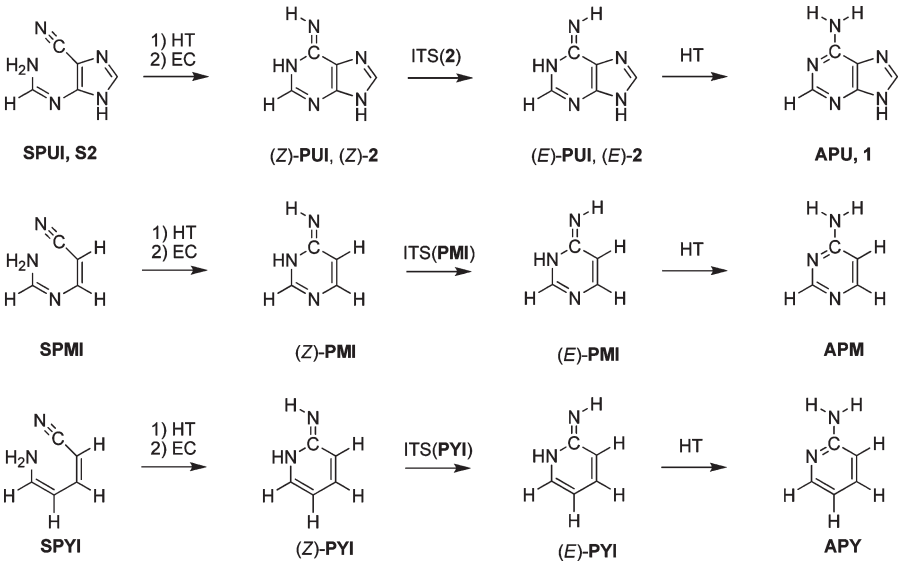

Smets and Meas studied 4-aminopyrimidine in argon matrices; they observed exclusively the amino tautomer, and their ab initio computations showed a preference of about 21.5 kcal/mol for **APM** over (*Z*)-**PMI** at the RHF/6-31++G(d,p) level.[2] Semiempirical computations by Öğretir and Yaman also showed a clear, albeit smaller preference of 14−15 kcal/mol for the amino tautomer **APM**.[3] Fujimoto et al. recently reported an (*E*)-preference energy of 2.9 kcal/mol for **PMI** based on using density functional computations at the B3LYP/6-311++G(d,p) level.[4] Regarding the pyridine system, computations by Hung et al. showed a preference of 14.1 kcal/mol of the amino tautomer **APY** over (*E*)-**PYI** at the B3LYP/6-31+G(d′,p′) level.[5] Hence, there is no doubt that the equilibria **PMI** ⇄ **APM** and **PYI** ⇄ **APY** lie on the side of the amino tautomer.[6] Whether equilibrium can be reached starting from the (*Z*)-imine depends on the reaction rates of the imine (*Z*)/(*E*)-isomerization (i.e., (*Z*)-**PMI** → (*E*)-**PMI**) and of the asymmetric amidine−amidine tautomerization (i.e., (*E*)-**PMI** → **APM**).

The (*Z*)/(*E*)-isomerization of imines can proceed with acid catalysis,[7] with base catalysis,[8,9] or with acid and base catalysis (i.e., via enamines).[10,11] In the present study, we are concerned with the uncatalyzed (*Z*)/(*E*)-isomerization. The barriers to (*Z*)/(*E*)-isomerization by way of *N*-inversion were measured for *N*-alkyl and *N*-aryl benzophenone imines (ArAr′C═N—R) in a number of seminal papers by Curtin et al.[12,13] (in cyclohexene, heptane, ethanol) and by Jennings et al.[14] (in diethyl ether, toluene, *tert*-butyl alcohol), and the activation energies are 17−30 kcal/mol depending on the arene substituents. Miller et al.[15] estimated the rate constant $k = 27\ s^{-1}$ at ca. 50 °C for the (*Z*)/(*E*)-isomerization of an R—CPh═N—Ph imine and this reaction rate corresponds to an activation barrier of $\Delta G^{\ddagger} = 16.8$ kcal/mol. The low inversion barriers of imines are in marked contrast to the high thermal stabilities of *N*-haloimines and of oximes. Inversion barriers of formimines H_2C═N—X (H, CN, F, OH) were studied by Bach et al.:[16,17] the computed barriers

(2) Smets, J.; Adamowicz, L.; Maes, G. Matrix-Isolation FT-IR Studies and ab-Initio Calculations of Hydrogen-Bonded Complexes of Molecules Modeling Cytosine or Isocytosine Tautomers. 2. 4-Aminopyridine and 4-Aminopyrimidine Complexes with H_2O in Ar Matrices. I. In *J. Phys. Chem.* **1995**, *99*, 6387–6400.

(3) Öğretir, C.; Yaman, M. AM1, PM3 and MNDO study of the tautomeric equilibria of 2-, 4- or 5-hydroxypyri-midin derivatives and their azo- and thio- analogs. In *THEOCHEM* **1999**, *458*, 217–226.

(4) Kitamura, T.; Okita, M.; Sasaki, Y.; Ishikawa, H.; Fujimoto, A. Amino-imino tautomerization reaction of the 4-aminopyrimidine/acetic acid system. In *Spectrochim. Acta A* **2008**, *69*, 350–360.

(5) Hung, F.-T.; Hu, W.-P.; Li, T.-H.; Cheng, C.-C.; Chou, P.-T. Ground and Excited-State Acetic Acid Catalyzed Double Proton Transfer in 2-Aminopyridine. In *J. Phys. Chem. A* **2003**, *107*, 3244–3253.

(6) Katritzky, A. R.; Pozharskii, A. F., Eds. *Handbook of heterocyclic chemistry*, 2nd ed.; Pergamon: New York, 2000; p 51.

(7) Johnson, J.; Morales, N.; Gorczyca, A.; Dolliver, D.; McAllister, M. For acid-catalyzed imine inversion, see for example: Mechanisms of Acid-Catalyzed Z/E Isomerization of Imines. In *J. Org. Chem.* **2001**, *66*, 7979–7985.

(8) For base-catalyzed imine inversion with deprotonation of imine-R, see for example: Cainelli, G.; Giacomini, D.; Trerè, A.; Boyl, P. Efficient Trans-amination under Mild Conditions: Preparation of Primary Amine Derivatives from Carbonyl Compounds via Imine Isomerization with Catalytic Amounts of Potassium *tert*-Butoxide. In *J. Org. Chem.* **1996**, *61*, 5134–5139.

(9) For base-catalyzed imine inversion with deprotonation at C_α, see for example: Gosselin, F.; Roy, A.; O'Shea, P.; Chen, C.; Volante, R. Oxazolidine Ring Opening and Isomerization to (E)-Imines. Asymmetric Synthesis of Aryl-α-fluoroalkyl Amino Alcohols. In *Org. Lett.* **2004**, *6*, 641–644.

(10) Morpurgoa, S.; Grandib, A.; Zazzab, C.; Bossa, M. A theoretical study on the sugars' mutarotation: the epimerization of 2-tetrahydropyranol catalysed by formamidine, benzamidine and by the 2-aminopyridine/2-iminopyridine tautomeric couple. In *THEOCHEM* **2005**, *729*, 71–82.

(11) Includes *E*/*Z*-isomerization via enamines: (a) Boyd, D. R.; Jennings, W. B.; Waring, L. C. Isomerization of Chiral Imines in [$^2H_4$]Methanol Solution. In *J. Am. Chem. Soc.* **1986**, *51*, 992–995. (b) Jennings, W.; Boyd, D. The Mechanism of Interconversion of (*Z*)- and (*E*)-Ketimines. In *J. Am. Chem. Soc.* **1972**, *94*, 7187–7188.

(12) Curtin, D.; Hausser, J. Effects of Structural Changes on the Interconversion of Stereoisomeric Imines. Isoelectronic Models for Vinyl Anions. In *J. Am. Chem. Soc.* **1961**, *83*, 3474–3481.

(13) Curtin, D. Y.; Grubbs, E. J.; McCarty, C. G. Uncatalyzed syn-anti Isomerization of Imines, Oxime Ethers, and Haloimines. In *J. Am. Chem. Soc.* **1966**, *88*, 2775–2786.

(14) Jennings, W.; Al-Showiman, S.; Boyd, D.; Campbell, R. Dynamic Stereochemistry of Imines and Derivatives. Part IX. The Mechanism of *E*-*Z* Isomerization in N-Alkylimines. In *J. Chem. Soc., Perkin II* **1976**, 1501–1506.

(15) Miller, S.; Reich, B.; Greenwald, E.; Justice, A.; Beckstead, B.; Reibenspies, J.; North, S. Phenyl-(2-phenylimino-1,2-diphenylethyl)-amine: Ene-diamine versus Imine-amine Isomeric Preferences. In *J. Org. Chem.* **2005**, *70*, 8409–8416.

(16) (a) Bach, R.; Wolber, G. Theoretical Study of the Barrier to Nitrogen Inversion in *N*-Cyano- and *N*-Diazoformimine. Mechanism of the Schmidt Reaction. In *J. Org. Chem.* **1982**, *47*, 239–245. (b) Bach, R.; Wolber, G. Theoretical Analysis of the Barrier to Nitrogen Inversion in *N*-Fluoroformimine and Formaldoxime. In *J. Org. Chem.* **1982**, *47*, 245–248.

(17) Bharatam, P.; Amita; Kaur, K. J. Electronic structure of *N*-sulfenylimines. In *Phys. Org. Chem.* **2003**, *16*, 183–188.

TABLE 1. Total Energies and Thermochemical Energies Computed with Perturbation Theory and Total Energies Computed with Coupled Cluster Theory

molecule	parameter[a]	(*E*)-isomerism	ITS	SOSP	(*Z*)-isomerization
PMI	*E*(MP2)[b]	−318.722047	−318.678401	−318.677034	−318.717093
	VZPE	59.77	57.96	57.40	59.50
	TE	63.13	61.38	60.71	62.90
	S	74.42	74.68	74.24	74.58
	NI	0	1	2	0
	ν_1	145	*i*1092	*i*1121	146
	ν_2	355	153	*i*353	348
	E(CC-L1)[c]	−318.725385	−318.679135	−318.678753	−318.720709
	E(CC-L2)[d]	−318.788523	−318.745161	−318.743961	−318.783723
	E(CC-L3)[e]	−318.937557	−318.894590	−318.893267	−318.932885
	E(CC-L4)[f]	−319.115963	−319.074460	−319.073597	−319.111370
PYI	*E*(MP2)[b]	−302.688281	−302.646233	−302.642207	−302.683717
	VZPE	66.72	65.13	64.41	66.48
	TE	70.25	68.61	67.88	70.04
	S	75.30	74.89	75.10	75.44
	NI	0	1	2	0
	ν_1	135	*i*1064	*i*1135	140
	ν_2	370	161	*i*473	359
	E(CC-L1)[c]	−302.695850	−302.650522	−302.648347	−302.691781
	E(CC-L2)[d]	−302.766813	−302.725082	−302.721643	−302.762516
	E(CC-L3)[e]	−302.907528	−302.866554	−302.862632	−302.903259
	E(CC-L4)[f]	−303.078133	−303.038261	−303.035128	−303.073925
PUI, **2**	*E*(MP2)[b]	−465.971644	−465.924304	−465.923667	−465.960512
	VZPE	70.80	68.75	68.29	70.41
	TE	75.25	73.34	72.70	74.90
	S	83.73	84.45	83.66	83.98
	NI	0	1	2	0
	ν_1	125	*i*1088	*i*1103	116
	ν_2	186	124	*i*299	194
	E(CC-L1)[c]	−465.955358	−465.905876	−465.905744	−465.944416
	E(CC-L2)[d]	−466.027965	−465.981121	−465.980525	−466.017008
	E(CC-L3)[e]	−466.280973	−466.234411	−466.234214	−466.270266
	E(CC-L3′)[g]	−466.280976	−466.235053	−466.234282	−466.270294
	E(CC-L4)[f]	−466.507668	−466.463021	−466.462916	−466.497371
	E(CC-L4′)[h]	−466.507762	−466.463398	−466.462988	−466.497485

[a]Total energies E_{tot} in atomic units, vibrational zero-point energies VZPE and thermal energies TE in kcal/mol, molecular entropies *S* in cal K^{-1} mol^{-1}, and frequencies in cm^{-1}. [b]MP2(full)/6-31G(d). [c]CCSD/6-31G(d). [d]CCSD/6-31+G(d). [e]CCSD(T)/6-311+G(d,p)//CCSD/6-31G(d). [f]CCSD(T)/6-311+G(2df,2p)//CCSD/6-31G(d). [g]CCSD(T)/6-311+G(d,p)//CCSD/6-31+G(d). [h]CCSD(T)/6-311+G(2df,2p)//CCSD/6-31+G(d).

fall in the wide range 15−60 kcal/mol and parallel experimental trends. *N*-inversion in exocyclic imines has not been studied.

Here we present the results of a theoretical study of the uncatalyzed, thermal *N*-inversion reactions of three 2-iminopyridines: pyrimidin-4(3*H*)-imine **PMI**, pyridin-2(1*H*)-imine **PYI**, and 1*H*-purine-6(9*H*)-imine **PUI**. Relevant regions of the potential energy surfaces were explored with Møller−Plesset perturbation theory and with coupled cluster theory. The results show a preference for the (*E*)-imine over its (*Z*)-isomer, and isomer preference energies and isomerization barriers were determined. Nonplanar *N*-inversion transition state (ITS) structures occur along enantiomeric reaction paths and structural parameters are defined to characterize the asymmetry of the ITS structures and to quantify the comparative analysis. The structural and the electronic relaxations along the entire *N*-inversion path of the isomerization (*Z*)-**PMI** ⇄ (*E*)-**PMI** were analyzed to elucidate the electronic origins of the asymmetry of the *N*-inversion paths.

Computational Methods

Potential energy surface (PES) analyses[18] were performed with second-order Møller−Plesset perturbation theory (MP2)[19,20] with all electrons included in the active space and in conjunction with the 6-31G(d) basis set. Stationary structures were optimized at this level, MP2(full)/6-31G(d), and vibrational analyses were performed at the same level. Total energies E_{tot}, vibrational zero-point energies (VZPE), thermal energies (TE), molecular entropies (*S*), the number of imaginary frequencies (NI), and the two lowest vibrational frequencies are provided in Table 1. In Table 2 are reported isomer preference energies, activation, and reaction energies. We report relative energies ΔE, enthalpies $\Delta H_0 = \Delta(E + \text{VZPE})$ and $\Delta H_{298} = \Delta(E + \text{TE})$, and free enthalpies $\Delta G = \Delta(E + \text{TE} - 298.15S)$.

While the thermochemical analysis of the isomers is sound, some caution is warranted with regard to the activation barriers because of the PES characteristics in the ITS regions. The imine-H vibration that displaces the hydrogen atom orthogonal to the transition vector for H-inversion (ν_{perp}) occurs in a double-well potential[21] with an extremely low barrier, i.e., $\Delta E_A \leq 0.5h\nu_{perp}$ (see Scheme 3). Consequently, the parameters VZPE(ν_{perp}) and TE(ν_{perp}) computed for the ITS structure with the harmonic approximation are somewhat overestimated. Local harmonic analysis of the SOSP structure becomes altogether irrelevant in this situation because the molecular motion along the deformation vector associated with ν_2 is a vibration.

(18) Cramer, C. J. *Essentials of Computational Chemistry*; Wiley: New York, 2004.
(19) Pople, J. A. Nobel lecture: Quantum chemical models. In *Rev. Modern Phys.* **1999**, *71*, 1267–1274.
(20) Wilson, S. *Handb. Mol. Phys. Quantum Chem.* **2003**, *2*, 314–373.
(21) Stanton, J, F. The quantum mechanics of atoms and molecules. In *Encyclopedia of Chemical Physics and Physical Chemistry*; Moore, J. H.; Spencer, N. D., Eds. Taylor & Francis: London, U.K., 2001; pp 3−47.

TABLE 2. Isomer Preference, Activation, and Reaction Energies

mol.	parameter[a,b]	ΔE_r for Z vs. E	ΔE_A for $E \rightarrow Z$	ΔE_A for $Z \rightarrow E$	ΔE_r for SOSP vs. ITS
PMI	ΔE(MP2)	3.11	27.39	24.28	0.86
	ΔH_0(MP2)	2.84	25.58	22.74	
	ΔH_{298}(MP2)	2.88	25.64	22.76	
	ΔG_{298}(MP2)	2.83	25.56	22.73	
	ΔE(CC-L1)	2.93	29.02	26.09	0.24
	ΔE(CC-L2)	3.01	27.21	24.20	0.75
	ΔE(CC-L3)	2.93	26.96	24.03	0.83
	ΔE(CC-L4)	2.88	26.04	23.16	0.54
	best estimate	2.60	24.21	21.61	
PYI	ΔE(MP2)	2.86	26.39	23.52	2.53
	ΔH_0(MP2)	2.62	24.80	22.17	
	ΔH_{298}(MP2)	2.65	24.75	22.09	
	ΔG_{298}(MP2)	2.61	24.87	22.26	
	ΔE(CC-L1)	2.55	28.44	25.89	1.36
	ΔE(CC-L2)	2.70	26.19	23.49	2.16
	ΔE(CC-L3)	2.68	25.71	23.03	2.46
	ΔE(CC-L4)	2.64	25.02	22.38	1.97
	best estimate	2.29	23.50	21.12	
PUI, 2	ΔE(MP2)	6.99	29.71	22.72	0.40
	ΔH_0(MP2)	6.60	27.66	21.06	
	ΔH_{298}(MP2)	6.64	27.80	21.26	
	ΔG_{298}(MP2)	6.56	27.58	21.02	
	ΔE(CC-L1)	6.87	31.05	24.18	0.08
	ΔE(CC-L2)	6.88	29.40	22.52	0.37
	ΔE(CC-L3)	6.72	29.22	22.50	0.12
	ΔE(CC-L3′)[c]	6.70	28.82	22.11	0.48
	ΔE(CC-L4)	6.46	28.02	21.56	0.07
	ΔE(CC-L4′)[c]	6.45	27.84	21.39	0.26
	best estimate	6.02	25.61	19.69	

[a]All data in kcal/mol. [b]See Table 1 for details on theoretical levels. [c]Energies based on CC-L2 optimized structures.

The potential energy surface analysis was refined by using variational coupled cluster theory considering all single and double excitations of the valence electrons.[22] The stationary structures were optimized at the levels CCSD/6-31G(d) and CCSD/6-31+G(d). The addition of diffuse function was thought important because diffuse functions improve the description of lone pairs and, more significantly, because lone pair density is altered in the course of an *N*-inversion reaction. The effects of triple excitations were examined with single-point energy computations with augmented valence triple-ζ basis sets and with use of CCSD optimized structures. For brevity, the theoretical levels CCSD/6-31G(d) and CCSD/6-31+G(d) are referred to as levels CC-L1 and CC-L2, respectively. The levels CCSD(T)/6-311+G(d,p) and CCSD(T)/6-311+G(2df,2p) are referred to as CC-L3 and CC-L4, respectively, when the energies are computed with the CCSD/6-31G(d) structures, and they are referred to as CC-L3′ and CC-L4′, respectively, when the energies are computed with the CCSD/6-31+G(d) structures.

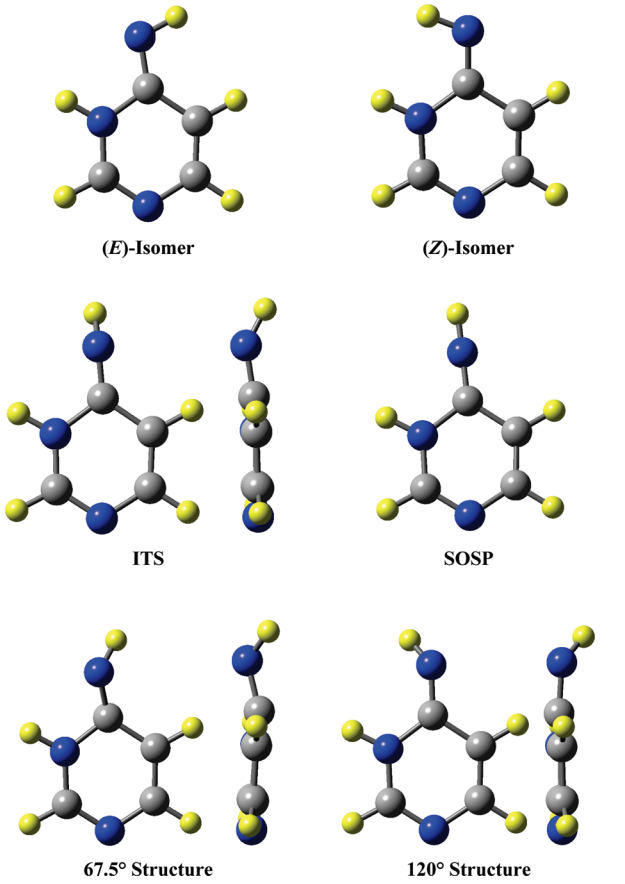

FIGURE 1. Molecular models of MP2(full)/6-31G(d) optimized structures of pyrimidin-4(3*H*)-imine, **PMI**.

The resulting total and relative energies are included in Tables 1 and 2, respectively.

Calculations were performed with Gaussian03[23] on a 64-processer SGI Altix system. GaussView[24] was employed as part of the analysis of the results and their display.

Results and Discussion

Isomers of Heteroarene Imines and *N*-Inversion. The heteroarene imines give rise to geometrical isomers, (*Z*)- and (*E*)-isomers, depending as to whether the imine-H and amino-N of the amidine moiety are on the same or opposite sides with respect to the C=N imine bond. The equilibrium structures of both isomers are planar for **PMI**, **PYI**, and **PUI**, and molecular models are shown in Figures 1−3, respectively.

Prasad et al. computed both geometrical isomers of the parent amidine HN=CH—NH_2 (formamidine, formimidamide), and reported a preference ΔE(MP2/6-31G(d)) = 1.6 kcal/mol for the (*E*)-isomer.[25] The (*E*)-isomer also is preferred for the heteroarene imines and the relative energies ΔE are 3.1 (**PMI**), 2.9 (**PYI**), and 7.0 (**PUI**) kcal/mol at the MP2

(22) Christiansen, O. Coupled Cluster Theory with Emphasis on Selected New Developments. In *Theor. Chem. Acc.* **2006**, *116*, 106–123.

(23) Frisch, M. J.; Trucks, G. W.; Schlegel, H. B.; Scuseria, G. E.; Robb, M. A.; Cheeseman, J. R.; Montgomery, J. A., Jr.; Vreven, T.; Kudin, K. N.; Burant, J. C.; Millam, J. M.; Iyengar, S. S.; Tomasi, J.; Barone, V.; Mennucci, B.; Cossi, M.; Scalmani, G.; Rega, N.; Petersson, G. A.; Nakatsuji, H.; Hada, M.; Ehara, M.; Toyota, K.; Fukuda, R.; Hasegawa, J.; Ishida, M.; Nakajima, T.; Honda, Y.; Kitao, O.; Nakai, H.; Klene, M.; Li, X.; Knox, J. E.; Hratchian, H. P.; Cross, J. B.; Bakken, V.; Adamo, C.; Jaramillo, J.; Gomperts, R.; Stratmann, R. E.; Yazyev, O.; Austin, A. J.; Cammi, R.; Pomelli, C.; Ochterski, J. W.; Ayala, P. Y.; Morokuma, K.; Voth, G. A.; Salvador, P.; Dannenberg, J. J.; Zakrzewski, V. G.; Dapprich, S.; Daniels, A. D.; Strain, M. C.; Farkas, O.; Malick, D. K.; Rabuck, A. D.; Raghavachari, K.; Foresman, J. B.; Ortiz, J. V.; Cui, Q.; Baboul, A. G.; Clifford, S.; Cioslowski, J.; Stefanov, B. B.; Liu, G.; Liashenko, A.; Piskorz, P.; Komaromi, I.; Martin, R. L.; Fox, D. J.; Keith, T.; Al-Laham, M. A.; Peng, C. Y.; Nanayakkara, A.; Challacombe, M.; Gill, P. M. W.; Johnson, B.; Chen, W.; Wong, M. W.; Gonzalez, C.; and Pople, J. A. *Gaussian 03*, Revision D.01; Gaussian, Inc., Wallingford, CT, 2004.

(24) Dennington, R., II; Keith, T.; Millam, J.; Eppinnett, K.; Hovell, W. L.; Gilliland, R. *GaussView*, Version 4.1; Semichem, Inc.: Shawnee Mission, KS, 2006.

(25) (a) Prasad, B.; Grover, G.; Uppal, P.; Kaur, D. *N*-Inversion and C−N Rotational Barriers in HX=CH—NH_2 (X = N, P, As) Compounds: an Ab Initio Study. In *THEOCHEM* **1999**, *458*, 227–237. (b) Note that "1-E, X = N" and "1-Z, X = N", respectively, are used in ref 25a to refer to the (Z)- and (E)-isomers, respectively.

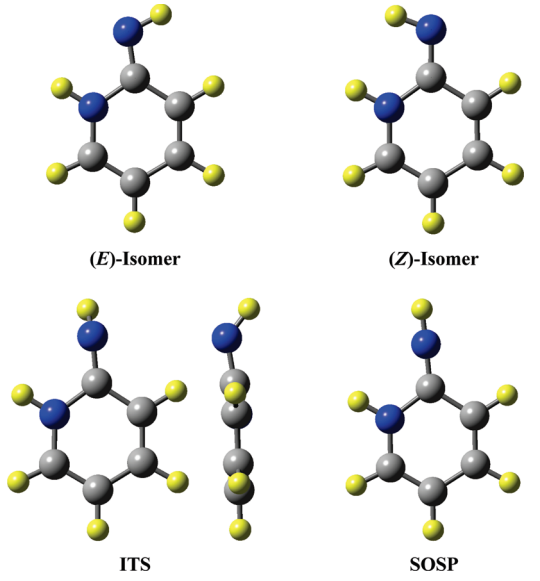

FIGURE 2. Molecular models of MP2(full)/6-31G(d) optimized structures of pyridin-2(1*H*)-imine, **PYI**.

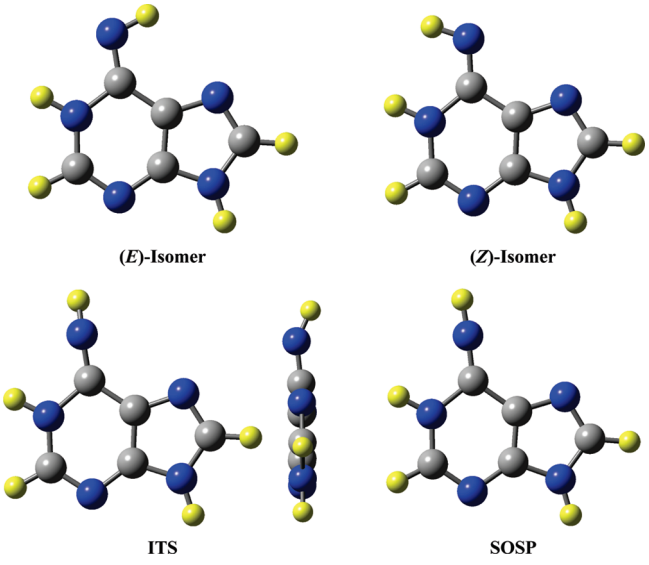

FIGURE 3. Molecular models of MP2(full)/6-31G(d) optimized structures of 1*H*-purine-6(9*H*)-imine, **PUI**, **2**.

level (Table 2). The (*E*)-preference for the purine stands out and suggests an extra stabilization of the (*E*)-isomer by way of intramolecular H-bonding between the imine H-donor and the N9-acceptor. Imine angles $\alpha = \angle(C-N-H)$ are collected in Table 3 and the data show that $\alpha(E)$ is about 2° smaller than $\alpha(Z)$ and that $\alpha(E)$ of **PUI** is somewhat smaller compared to **PMI** and **PYI**.

It is one reasonable possibility that the transition state structure for *N*-inversion also is planar. Hence, the respective stationary structures were located in the region $\alpha \approx 180°$ and they were found to correspond to second-order saddle points, SOSP. For **PMI**, for example, the imaginary mode $\nu_1 = i1121$ cm^{-1} corresponds to atom displacements expected for the transition vector for in-plane *N*-inversion, and the second imaginary mode $\nu_2 = i353$ cm^{-1} corresponds mostly to an out-of-plane displacement of the imine-H. The

SCHEME 2. Atom Numbering and Definitions of Angles $\alpha = \angle(C-N-H)$ and $\beta = \angle(X_C-N-H)$

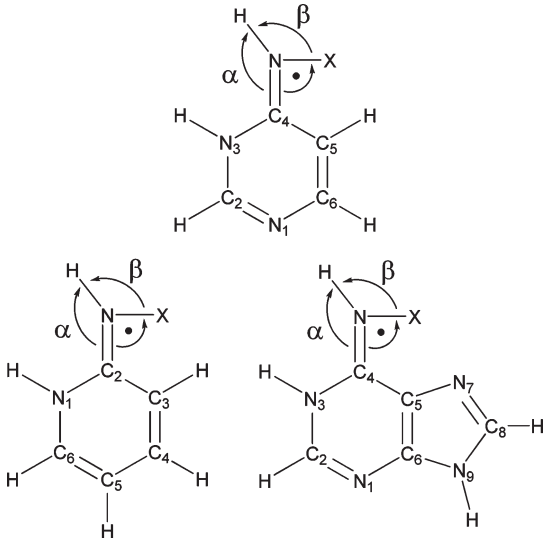

TABLE 3. Imine Angles and Nonplanarity of *N*-Inversion Transition State Structures[a,b]

		α			ITS			
method	mol.	*Z*	*E*	SOSP	α	β	η	σ
MP2	**PMI**	111.5	109.2	179.1	143.6	94.2	216.4	171.4
	PYI	111.2	109.4	179.2	133.0	95.7	226.7	170.7
	PUI	111.3	108.3	177.4	149.2	95.1	210.4	172.4
CC-L1	**PMI**	111.5	109.7	179.2	151.2	93.0	208.7	172.5
	PYI	111.2	109.6	179.3	135.9	95.0	223.8	170.8
	PUI	111.3	108.7	177.5	180.0	90.0	180.0	180.0
CC-L2	**PMI**	111.7	110.0	179.2	144.4	94.1	215.4	170.9
	PYI	111.5	109.9	179.3	132.9	95.7	226.8	170.4
	PUI	111.5	109.3	177.4	150.3	95.1	209.3	172.1

[a]MP2: MP2(full)/6-31G(d). CC-L1: CCSD(fc)/6-31G(d). CC-L2: CCSD(fc)/6-31+G(d). [b]All values in degrees.

actual transition state structures were located in searches that started with a nonplanar trial structure generated by an out-of-plane displacement of the imine-H. The resulting stationary inversion transition state structure, ITS, exhibited just one imaginary mode as they should. In the case of ITS(**PMI**), for example, the one imaginary mode with frequency $\nu_1 = i1093$ cm^{-1} featured the expected transition vector for *N*-inversion. We expected that the vibration with the lowest (real) frequency, i.e., $\nu_2 = 153$ cm^{-1} for **PMI**, would correspond mostly to an out-of-plane displacement of the imine-H atom. However, ν_2 now shows a skeletal motion that moves the entire NH-group out of the plane and that is even dragging the imine-C along in the same direction. The ITS structures feature α angles that are much larger than the sp^2 hybridization angle and clearly the angles are nowhere near 180° either. In addition to the imine-H, the imine-N also is out of the best plane of the heteroarene in the ITS structures, and the imine-N and the imine-H are on opposite faces of the heteroarene in all cases (Figures 1−3).

The imine angle $\alpha = \angle(C-N-H)$ is a good reaction coordinate to describe the all-in-plane *N*-inversion between the imine isomers, (*Z*)-isomer $\alpha < 180°$ and (*E*)-isomer $\alpha > 180°$, so long as it is defined in what direction the angle is to be measured (i.e., clockwise when viewed from the *Re* face). It is advantageous to describe the nonplanar *N*-inversion

SCHEME 3. Enantiomeric Paths for *N*-Inversion Connect the Isomeric Minima (Dashed Lines)[a]

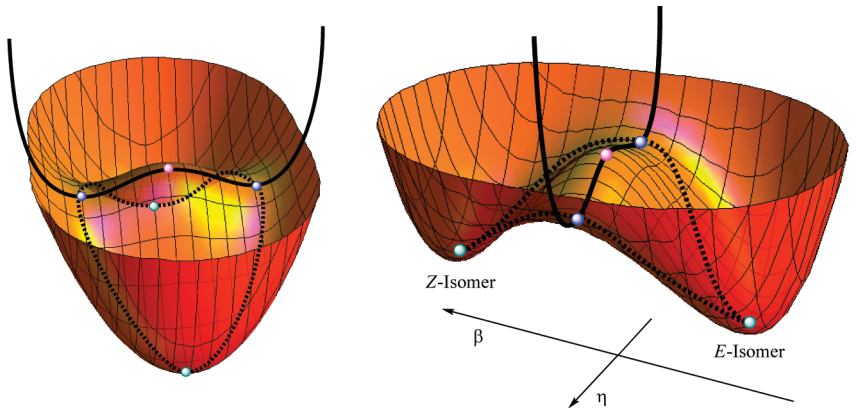

[a]The out-of-plane motion of the imine-H (η) occurs in a double-well potential (solid curve) with an extremely low-energy barrier.

using the angle $\beta = \angle(X_C{-}N{-}H)$ as the reaction coordinate, and we select the placement of X such that it is on the side of C5 and in the (N,C4,C5)-plane for **PMI** (Scheme 2). With this choice of reference, one can now define the dihedral angle $\eta = \angle(H{-}N{-}X_C{-}C4)$ as a measure of the displacement of the imine-H out of the (N,C4,C5)-plane. Further, we employ the dihedral angle $\sigma = \angle(N{-}C4{-}C5{-}N1)$ to quantify the displacement of the imine-N out of the (C4,C5,N1)-plane ($\sigma \neq 180°$). The parameters are defined in complete analogy for **PYI** and **PUI**, and all data are collected in Table 3.

The data in Table 3 show that the three heteroarene imines exhibit similar movements of the imine-N out of the plane of the heteroarene, with σ values of 170−172°, and most of the variability of the imine angle reflects changes in the dihedral angle η. Scheme 3 illustrates the potential energy surface as a function of the coordinates β and η. The enantiomeric paths for *N*-inversion and the double-well potential orthogonal to the transition vectors are indicated.

To ensure that the structural features of the MP2-PES are real, we thought it important to explore the potential energy surfaces with coupled cluster theory. We optimized the isomers and the planar and nonplanar saddle point structures using coupled cluster theory CCSD and with the basis sets 6-31G(d) and 6-31+G(d). The same structural characteristics occur at levels CC-L1 and CC-L2 for the imines **PMI** and **PYI**, but theoretical level dependencies occur for **PUI**, and the purine imine benefits the least from nonplanarity at the MP2/6-31G(d) level. The ITS and SOSP structures of **PUI** essentially coalesce at the CC-L1 level, whereas the addition of diffuse functions to the basis set recovers the benefits of nonplanarity of **PUI** at the CC-L2 level. Clearly, still better theoretical levels were needed to reach a conclusion regarding the topology of the inversion transition state region of **PUI** and we employed CCSD(T) theory in conjunction with the much larger basis sets 6-311+G(d,p) and 6-311+G(2df,2p). The CCSD(T) energies were computed with the CCSD/6-31G(d) structures, i.e., levels CC-L3 and CC-L4, for **PMI**, **PYI**, and **PUI**. The choice of structure used in the CCSD(T) computations does matter for **PUI**, of course, and we computed CCSD(T)/6-311+G(d,p) and CCSD(T)/6-311+G(2df,2p) energies for all stationary structures of **PUI** also with the CCSD/6-31+G(d) structures, i.e., at levels CC-L3′ and CC-L4′. The relative energies between ITS(**PUI**) and SOSP(**PUI**) suggest that there are stationary points that formally correspond to nonplanar transition state structures and that there exists a wide transition state region between them that is easily accessible.

At the MP2 level, the *E*-preference energies $\Delta E(Z$ vs. $E)$ are 3.1 (**PMI**), 2.9 (**PYI**), and 7.0 (**PUI**) kcal/mol, the activation barriers $E_A(Z \rightarrow E)$ are 24.3 (**PMI**), 23.5 (**PYI**), and 22.7(**PUI**) kcal/mol, and the nonplanar ITS structure is preferred over the respective SOSP structure by 0.9 (**PMI**), 2.5 (**PYI**), and 0.4 (**PUI**) kcal/mol. Accounting for thermochemistry results in slightly lower *E*-preference free enthalpies $\Delta G_{298}(Z$ vs. $E)$ of 2.8 (**PMI**), 2.6 (**PYI**), and 6.6 (**PUI**) kcal/mol and also in slightly lower free enthalpies of activation $\Delta G_{298}(Z \rightarrow E)$ of 22.7 (**PMI**), 22.3 (**PYI**), and 21.0 (**PUI**) kcal/mol. The "best estimates" in Table 2 are based on energies computed at the levels CC-L4 (**PMI**, **PYI**) and CC-L4′ (**PUI**) and thermodynamic parameters computed at the MP2(full)/6-31G(d) level. The best estimates for the (*E*)-preference free enthalpies $\Delta G_{298}(Z$ vs. $E)$ are 2.6 (**PMI**), 2.3 (**PYI**), and 6.0 (**PUI**) kcal/mol and for the free enthalpies of activation $\Delta G_{298}(Z \rightarrow E)$ they are 21.6 (**PMI**), 21.1 (**PYI**), and 19.7 (**PUI**) kcal/mol.

Imine-Polarization and Isomerization. Pertinent results of NBO[26] charge distribution analyses of the (*E*)- and (*Z*)-isomers of **PMI** and of the saddle point structures ITS(**PMI**) and SOSP(**PMI**) are shown in Figure 4. Atom charges are illustrated by using a symmetric color range from red (−0.9) to green (+0.9) with bright color indicating charge centers and shaded colors representing less polar regions. The amidine moiety R—NH—C(=NH)—R′ is the dominant polar motif within pyrimidin-4(3*H*)-imine. The numbers in parentheses refer to the charges of the NH groups and the data show that the exocyclic C=NH moiety is highly polarized. Comparison of the data for the equilibrium and the saddle point structures (Figure 4) shows that isomerization requires *additional* polarization of the already highly polar imine bond and this very fact is the fundamental origin of the isomerization barrier.

(26) (a) Weinhold, F. Natural bond orbital methods. In *Encyclopedia of Computational Chemistry*; Schleyer, P. v. R., Allinger, N. L., Clark, T., Gasteiger, J., Kollman, P. A., Eds.; Wiley: Chichester, UK, 1998; Vol. 3, pp 1792−1811. (b) Weinhold, F.; Landis, C. R. Natural bond orbitals and extensions of localized bonding concepts. In *Chem. Educ.: Res. Pract. Eur.* **2001**, *2*, 91–104.

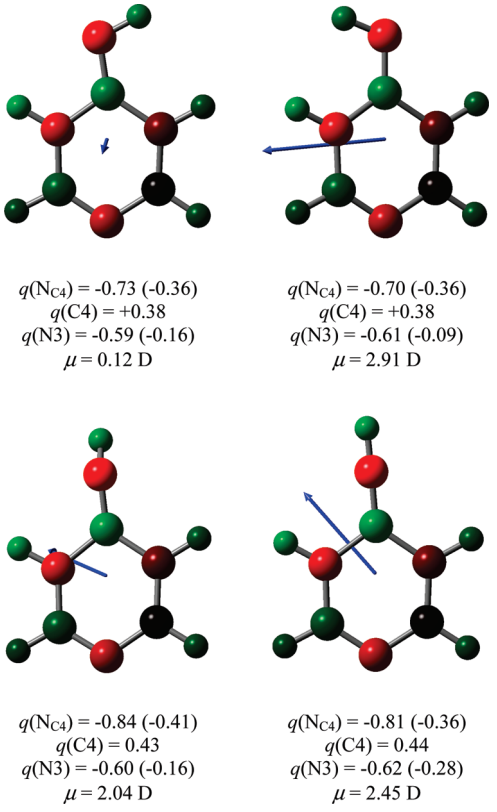

FIGURE 4. The charge distributions are illustrated using a linear color scale −0.9 (red) ≤ q ≤ 0.9 (green) for the (*E*)- and (*Z*)-isomer of **PMI** and the saddle point structures **ITS** and **SOSP**. Blue arrows illustrate the molecular dipole moments and they are drawn to scale (except for (*E*)-**PMI**, which is shown three times larger).

If the additional polarization of the already highly polar imine bond is the cause of the isomerization barrier, then one should expect the inversion barrier to correlate with the ability of *N*-substituents to accommodate excess charge. Studies by Bach and Wolber support this notion in that inversion barriers computed that the RHF/6-31G level for a series of formimines $H_2C{=}N{-}X$ follow the order 14.4 (X = CN), 25.2 (X = H), 77.4 (X = F), and 59.5 kcal/mol X = (OH).[16] The *N*-inversion barrier of sulfeneimine also fits this notion in that sulfur's d-orbitals can delocalize excess density. For the parent sulfeneimine, $H_2C{=}N{-}SH$, inversion barriers $\Delta H_0^{\ddagger}$ were reported of 24.6 and 20.8 kcal/mol at MP2(full)/6-31+G(d) and CBS-Q, respectively.[17]

A rotation process is the worst-case scenario in terms of overall charge accumulation on the NH moiety with the only advantageous feature of allowing for minimization of repulsion between the N-lone pairs (sp^2 to sp^3; i.e., **C** in Scheme 4). Most importantly, the inversion process (sp^2 to sp) does *not* avoid up-polarization of the imine bond and representations of type **B** are really quite misleading. But the inversion offers an alternative mode for the distribution of the excess electron density at the imine-N (form **D**) while enabling at least some contribution from **B**. The up-polarization of the exocyclic CN bond does not have a major consequence on the in-ring amidine bond (Figure 4) and structures of type **C**′ and **D**′ are no more important during (*E*)/(*Z*)-isomerization than in the minima. Generally, one would assume any back-donation from N to be most effective so long as the p_π-type density of

SCHEME 4. Diagram of How Much Charge Is on Nitrogen

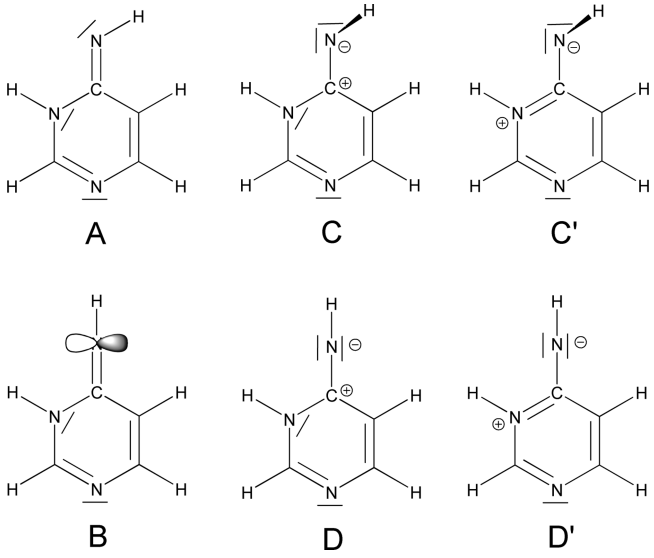

the imine-N is most aligned with the π-system of the heterocycle (i.e., **A**, **B**) and one would further assume that any such back-donation should be stronger in the ITS than in the equilibrium structures. Yet, this reasoning creates somewhat of a paradox because the ITS structures show that the imine group is decidedly nonlinear and, moreover, that the imine-N atom does not remain coplanar with the heterocycle. It was this observation that stimulated our study and we will suggest a resolution of this conflict.

***N*-Inversion Energy Profile and Structural Relaxation.** It is advantageous to describe the nonplanar *N*-inversion by using the angle $\beta = \angle(X_C{-}N{-}H)$ as the reaction coordinate (Scheme 2). The isomerization of the (*E*)- to the (*Z*)-isomer of **PMI** corresponds to a change of β from 19.6° to 158.5°, and we studied the inversion energy profile of **PMI** as a function of β with and without imposed planarity. The inversion energy profiles are shown in Figure 5. The blue curve $E(C_s)$ represents in-plane inversion and the red curve $E(C_1)$ allows for nonplanar structures along the inversion path. The green curve shows the relative stabilization of the nonplanar structure for a given β angle, $\Delta E_{def} = E(C_s) - E(C_1)$. The deformation energies are small (< 1 kcal/mol) at the locations of the stationary points and along the ascent from the (*Z*)-isomer to the transition state structure ITS(**PMI**), but ΔE_{def} values are substantial in the region of the ascent from the (*E*)-isomer to ITS(**PMI**) with a maximum of $\Delta E_{def}(67.5°)$ = 5.3 kcal/mol.

Pertinent parameters describing the structural relaxation along the inversion reaction are shown in Figure 6. The imine angle $\alpha = \angle(C{-}N{-}H)$ serves as a proxy for *N*-hybridization, it is about 120−130° along most of the path, and its value never exceeds 150° even in the transition state region. The purple curve shows $\eta = \angle(H{-}N{-}X_C{-}C4)$, the dihedral angle that measures the displacement of the imine-H out of the (N,C4,C5)-plane. The golden curve shows the dihedral angle $\sigma = \angle(N{-}C4{-}C5{-}N1)$, the parameter that quantifies the displacement of the imine-N out of the (C4,C5,N1)-plane ($\sigma \neq 180°$). Angles $\sigma > 180°$ are used to indicate that both atoms of the NH moiety are on the same side of the best plane of the heterocycle. Figure 6 shows that the changes of η and

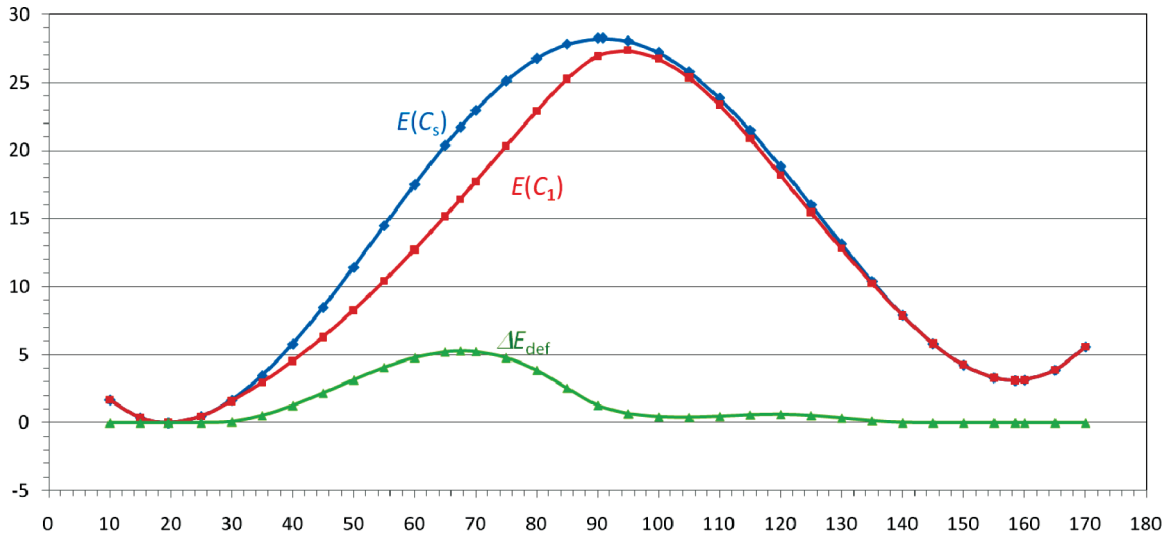

FIGURE 5. Discretized inversion energy profile as a function of angle $\beta = \angle(X_C{-}N{-}H)$. Energies are in kcal/mol relative to the (*E*)-isomer. The (*E*)- and (*Z*)-minima appear on the left and right, respectively. The blue curve $E(C_s)$ represents in-plane inversion while the red curve $E(C_1)$ allows for nonplanar structures along the inversion path. The green curve $\Delta E_{def} = E(C_s) - E(C_1)$ shows the relative stabilization of the nonplanar structure for a given angle β. The "amidine effect" is largest in the ascent region from the (*E*)-isomer to ITS.

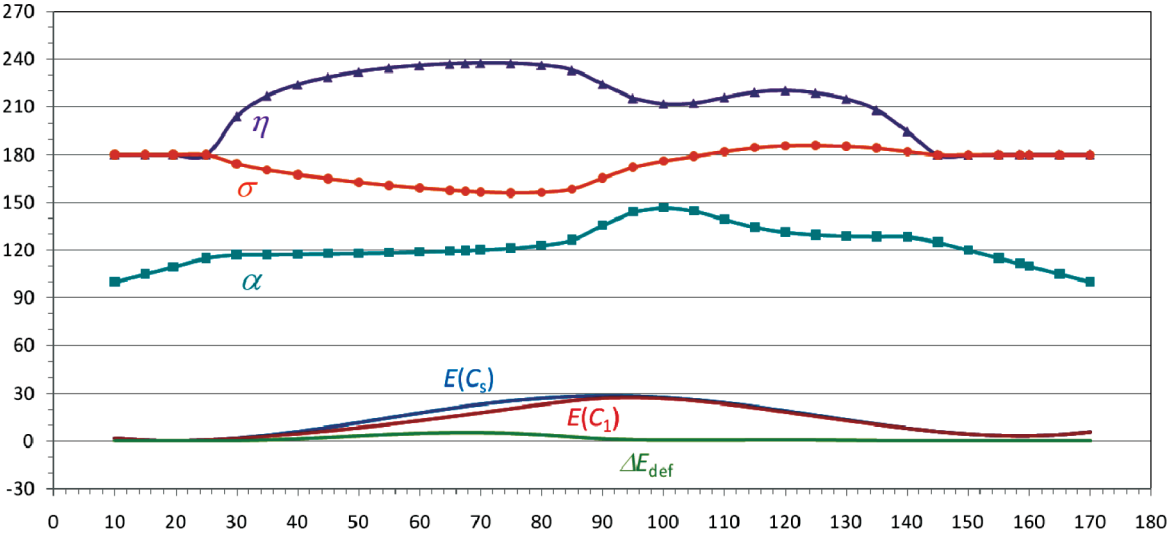

FIGURE 6. Angles and dihedral angles (in degrees) of structures along the inversion paths as a function of angle $\beta = \angle(X_C{-}N{-}H)$. Discretized inversion energy profiles (in kcal/mol) are included for orientation. The turquoise curve shows $\alpha = \angle(C{-}N{-}H)$ and serves as a proxy for *N*-hybridization. The purple curve shows $\eta = \angle(H{-}N{-}X{-}C4)$ and measures the displacement of the imine-H out of the NC4C5-plane. The golden curve shows $\sigma = \angle(N{-}C4{-}C5{-}N1)$ and measures the displacement of the imine-N out of the C4C5N1-plane.

σ are in-phase in the ascent region from the (*Z*)-isomer toward the ITS region. In contrast, these dihedrals are out-of-phase in the ascent region from the (*E*)-isomer toward the ITS region and the transition state structure ITS(**PMI**) falls in this region (Figure 1). This type of out-of-plane deformation is most pronounced in the region $60° < \beta < 80°$ (i.e., the 67.5° structure).

MO-Analysis of Electronic Relaxation. Molecular orbital theory provides an explanation of the electronic feature that causes these distinct types of structural relaxations along the flanks of the inversion barrier. We analyzed the electronic structure of the 67.5° structure of **PMI** where the effects are most clearly revealed, and surface plots of some relevant MOs are shown in Figure 7. We also analyzed the electronic effects of the 120° structure, which is essentially indifferent to out-of-plane deformation, and surface plots of its analogous MOs are shown in Figure 8.

The molecular orbitals of pyrimidin-4(3*H*)-imine can be constructed by a combination of the pyrimidine $2b_1$- and $1a_2$-type MOs[27] with the fragment MOs (FMO) of the NH moiety. MO22 (π_3) is the bonding combination of the NH-group's p-type FMO and the pyrimidine π_2-type MO. The node plane cuts through the N1−C2 and N3−C4 bonds and the NH-group's p_π-type FMO allows for overlap between the imine moiety and the heterocycle. The essential characteristics of this MO are retained in the nonplanar 67.5°

(27) Ning, C. G.; Liu, K.; Luo, Z. H.; Zhang, S. F.; Deng, J. K. Electron momentum spectroscopy study on valence electronic structures of pyrimidine. In *Chem. Phys. Lett.* **2009**, *476*, 157–162.

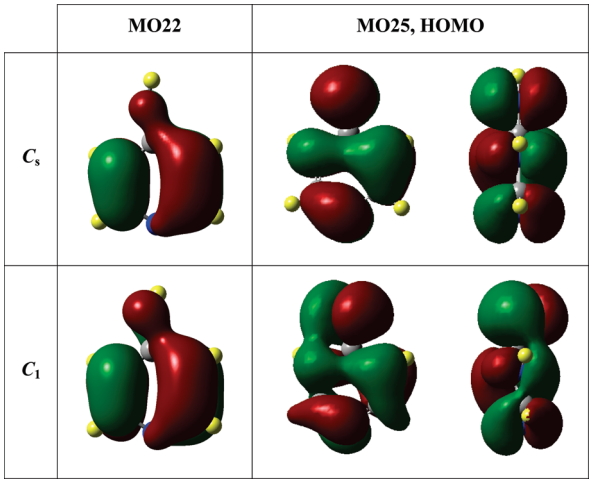

FIGURE 7. Surface plots of MO22 (left) and two perspectives of MO25 (HOMO) of the $\beta = 67.5°$ structures for in-plane inversion (top) and allowing for oop-deformation (bottom).

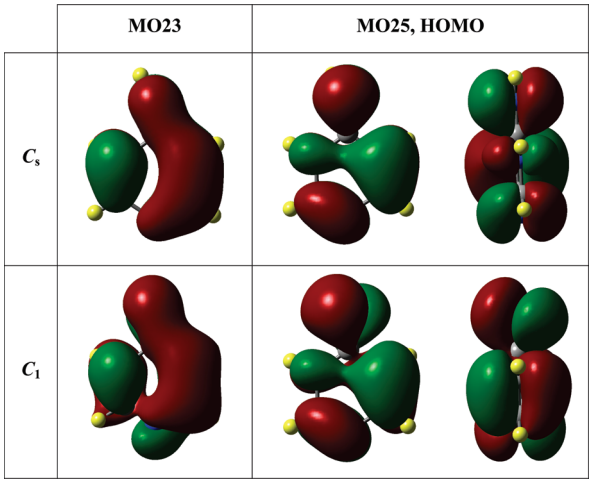

FIGURE 8. Surface plots of MO23 (left) and two perspectives of MO25 (HOMO) of the $\beta = 120°$ structures for in-plane inversion (top) and allowing for oop-deformation (bottom).

structure. MO25 (π_4), the HOMO, is formed by the antibonding combination of the NH-group's p_π-type FMO and the pyrimidine π_3-type MO. The out-of-plane deformation of the imine moiety does have a significant effect on the HOMO in that it creates two additional overlaps (Figure 7) and both of these overlaps occur between lopes on opposite faces of the best plane of the heterocycle: Major overlap occurs between the imine-N and N3 (primary overlap) and a smaller (secondary) overlap occurs between N3 and C2. Hence, the oop-deformation allows for more delocalization of electron density. The extra stabilization of the nonplanar structure by this effect should be most effective when the dihedral angles η and σ are out-of-phase.

Asymmetry and ITS Structures. The isosurface plots in Figure 9 show the HOMOs of ITS(**PMI**), ITS(**PYI**), and ITS(**PUI**) and they were generated with the value of the electron density set to half of the value used for the plots of Figures 7 and 8. While the extra delocalization is strongest in the (*E*)-**PMI** → ITS(**PMI**) ascent region, the inversion energy profile of Figure 5 shows that the effect remains strong

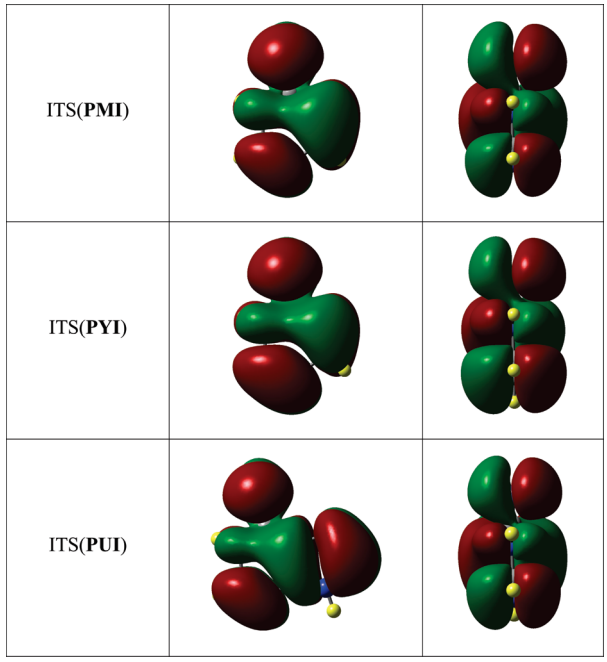

FIGURE 9. Surface plots in two perspectives of HOMO of the ITS structures of pyrimidin-4(3*H*)-imine (MO25, top), pyridin-2(1*H*)-imine (MO25, center), and 1*H*-purine-6(9*H*)-imine (MO35, bottom). The isosurfaces are drawn for an electron density value that is one-half of the value used for the generation of the plots in Figures 7 and 8.

enough in the transition state region to cause a small shift of ITS(**PMI**) *toward* the (*Z*)-isomer relative to SOSP(**PMI**). The additional overlap in the region between the imine-N and N3 is much less pronounced compared to the 65° structure, but the ridge of overlap remains clearly visible. The second, minor overlap that occurs in the region between N3 and C2 of the 65° structure has all but vanished in the ITS structure.

Because the discussed effect is strongest in the (*E*)-Isomer → ITS ascent region, one should expect[28] that a comparable imine with a smaller or higher (*E*)-preference should benefit more or less strongly from this effect, respectively. The results for pyridin-2(*1H*)-imine and purine-6(9*H*)-imine support this line of thought. The expectation is most fully borne out for **PYI**. *N*-Inversion scenarios of **PMI** and **PYI** are similar in that the (*E*)/(*Z*)-isomerizations of both imines proceed via a pair of chiral inversion transition state structures ITS (Figures 1 and 2), their structural features are similar and the dihedral angles η and σ are out-of-phase, and the computed ΔE_r(SOSP vs. ITS) values (Table 2) show that **PYI** benefits about three times as much from nonplanarity as compared to **PMI**. The HOMO of ITS(**PYI**) shows a stronger ridge of overlap across the in-ring amidine bond (Figure 9). Considering the relative isomer stabilities, one would expect the transition state structure for the *N*-inversion (*Z*)-**PUI** → (*E*)-**PUI** to occur earlier along the inversion path compared to either **PMI** or **PYI**. The presence of N9 in **PUI** provides an incentive for back-donation in the HOMO that is not present in **PMI** or **PYI**. Inspection of Figure 9 shows that delocalization occurs in the

(28) Bulat, F. A.; Toro-Labbe, A. An Extension of the Hammond Postulate. Structural Effects on the Classification of Chemical Reactions. In *J. Phys. Chem. A* **2003**, *107*, 3987–3994.

TABLE 4. Computed Solvation Effects on Isomer Preference, Activation, and Reaction Energies of PMI

mol.	parameter[a]	ΔE_r for Z vs. E	ΔE_A for $E \rightarrow Z$	ΔE_A for $Z \rightarrow E$	ΔE_r for SOSP vs. ITS
PMI$_{gas}$	ΔE	3.11	27.39	24.28	0.86
	ΔH_0	2.84	25.58	22.74	
	ΔH_{298}	2.88	25.64	22.76	
	ΔG_{298}	2.83	25.56	22.73	
PCM($HCCl_3$)	ΔE	1.77	27.91	26.14	1.37
	ΔH_0	1.59	25.95	24.35	
	ΔH_{298}	1.62	26.01	24.39	
	ΔG_{298}	1.58	25.92	24.34	
PMI·$ClCH_3$	ΔE	4.73	26.95	22.23	1.04
	ΔH_0	4.28	25.18	20.90	
	ΔH_{298}	4.40	25.22	20.82	
	ΔG_{298}	3.46	25.30	21.84	

[a]All data in kcal/mol and computed at MP2(full)/6-31G(d).

HOMO of ITS(**PUI**) and that the effect is the least pronounced among the three imines.

Solvent Effects on *N*-Inversion. The results presented show that there are no intrinsic reasons to prevent nonplanar *N*-inversion paths in the gas phase. Naturally, the question arises as to whether this conclusion might carry over to solution chemistry. We presented evidence to support the notion that isomerization requires additional polarization of the already highly polar imine bond. Hence, solvents of low polarity (i.e., $HCCl_3$, $\varepsilon = 4.9$) might be expected to resist the up-polarization, to increase the *N*-inversion barrier, and to retain the asymmetry of the *N*-inversion path, whereas polar solvents might facilitate the up-polarization, reduce the *N*-inversion barrier, and perhaps even facilitate essentially an in-plane *N*-inversion. The results of an initial solvation study of *N*-inversion of **PMI** with Tomasi's polarized continuum model[29] at the PCM(MP2(full)/6-31G(d)) level corroborate these expectations (Table 4). On the other hand, the nature of the solvent undoubtedly will affect the structural characteristics of the isomerization path because of specific solute−solvent interactions. Chlorinated solvents, for example, engage in halogen bonding, that is, an intermolecular attraction between an organic halide R−X and a highly electronegative atom such as an imine-N.[30,31] Preliminary studies of the halogen-bonded aggregate **PMI**·$ClCH_3$ at the MP2-(full)/6-31G(d) level suggest that halogen bonding enhances the (*E*)-preference energy, increases the asymmetry of the inversion transition state structure, and decreases the *N*-inversion barrier (Table 4). The solvent molecule interacts with the amidine moiety by way of halogen bonding and hydrogen bonding in (*E*)-**PMI**·$ClCH_3$, whereas only one halogen-bonding interaction occurs in (*Z*)-**PMI**·$ClCH_3$ (Figure 10). This difference in the mode of aggregation causes the enhanced (*E*)-preference energy for **PMI**·$ClCH_3$, and **ITSa** is more stable than **ITSb** for the same reason. Clearly, larger aggregates **PMI**·$(ClCH_3)_n$ (possibly embedded in a polarizable continuum) need to be studied to better understand the solvent effects on isomer preferences and inversion energies of imines. The initial studies suggest that the asymmetry in *N*-inversion paths is retained and perhaps even enhanced in chlorinated solvents of low polarity.

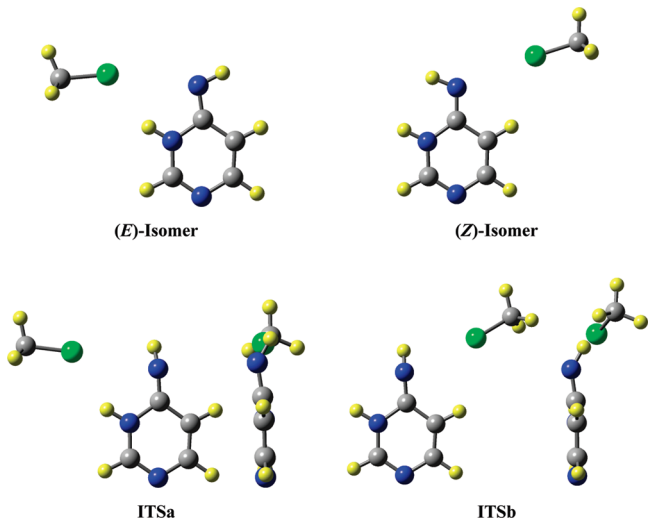

FIGURE 10. Molecular models of MP2(full)/6-31G(d) optimized structures of halogen-bonded aggregates of pyrimidin-4(3*H*)-imine and chloromethane, **PMI**·$ClCH_3$.

Conclusion

The best estimates for the (*E*)-preference free enthalpies ΔG_{298}(*Z* vs. *E*) are 2.6 (**PMI**), 2.3 (**PYI**), and 6.0 (**PUI**) kcal/mol and for the free enthalpies of activation $\Delta G_{298}(Z \rightarrow E)$ the best estimates are 21.6 (**PMI**), 21.1 (**PYI**), and 19.7 (**PUI**) kcal/mol. The pre-exponential factors for thermal isomerizations of alkenes, imines, and diazenes[32] are on the order of $10^{13}-10^{14}$ and, hence, the computed activation barriers translate into half-lives on the order of 0.1−10 s at room temperature, of 1−50 min at −20 °C, and into many months and years at temperatures below −100 °C. Under typical laboratory chemical condition the thermal equilibration of these exocyclic imines is very fast and both isomers are readily available for reactions. The thermal isomerization obviously is shut down in cold gas-phase scenarios (ISM, dark molecular clouds, 10−25 K), whereas models of hot core evolution and of protoplanetary disk (PPD) chemistry suggest that temperatures in the inner region (< 5 AU) allow for effective thermal isomerization.[33,34]

The discussion of the asymmetry along the *N*-inversion processes in the heteroarene imines points out the very possibility for the occurrence of enantiomeric *N*-inversion paths. It is true that the energy differences ΔE_{def} between the chiral TS structure and the respective planar SOSP structure are small in all cases. But it is also true that the difference $\Delta E_{def} \approx 2$ kcal/mol for **PYI**, for example, cannot be

(29) Tomasi, J.; Mennucci, B.; Cammi, R. Quantum mechanical continuum solvation models. In *Chem. Rev.* **2005**, *105*, 2999–3093.
(30) (a) Metrangolo, P.; Resnati, G. Halogen versus Hydrogen. In *Science* **2008**, *321*, 918–919. (b) Karpfen, A. Theoretical characterization of the trends in halogen bonding. In *Struct. Bonding* (*Berlin*) **2008**, *126*, 1–15.
(31) (a) Glaser, R.; Murphy, R. F. What's in a name? Noncovalent Ar-Cl···(H-Ar′)$_n$ interactions and terminology based on structure and nature of the bonding. In *CrystEngComm* **2006**, *8*, 948–951. (b) Glaser, R.; Chen, N.; Wu, H.; Knotts, N.; Kaupp, M. ^{13}C-NMR Study of Halogen Bonding of Haloarenes. Measurement of Solvent Effects and Theoretical Analysis. In *J. Am. Chem. Soc.* **2004**, *126*, 4412–4419.
(32) Jeffers, P. M.; Shaub, W. Shock Tube cis-trans Isomerization Studies. In *J. Am. Chem. Soc.* **1969**, *91*, 7706–7709.
(33) Shaw, A. M. *Astrochemistry*; Wiley: Chichester, U.K., 2006; p 113ff.
(34) (a) Millar, T. J.; Nomura, H.; Markwick, A. J. Two-Dimensional Models of Protoplanetray Disk Chemistry. In *Astrophysics and Space Science* **2003**, *285*, 761–768. (b) Garrod, R. T.; Herbst, E. Formation of methyl formate and other organic species in the warm-up phase of hot molecular cores. In *Astron. Astrophys.* **2006**, *457*, 927–936.

dismissed because its magnitude is such that the asymmetry effect will be reflected in experimental measurements. Halogenated solvents can engage in strong halogen bonding with imines and amide-type transition state structures. The discussion of the halogen-bonded aggregate **PMI**·$ClCH_3$ exemplifies that the asymmetry in *N*-inversion paths is retained and perhaps even enhanced in chlorinated solvents of low polarity.

The detailed study of structures and electronic structures along the entire *N*-inversion path of the isomerization (*Z*)-**PMI** ⇄ (*E*)-**PMI** revealed the special benefits of asymmetry in the ascent region from the (*E*)-isomer to ITS(**PMI**) with a remarkable maximum of $\Delta E_{def}^{max} = 5.3$ kcal/mol. Structures in this region of the potential energy surface allow best for additional bonding overlaps in the HOMO and even a small shift of the ITS toward that region would garner noticeable benefit. This result has rather practical implications in that the theoretical insight leads directly to the prediction of lower *N*-inversion barriers in analogous imines with (*Z*)-preference energies (i.e., N3-, N(C4)-, and/or C5-substituted **PMI** derivatives). We believe this effect to present a characteristic feature of the amidine motif present in all of the heteroarene imines studied, that is, we predict this same effect to occur in other heteroaromatic systems that incorporate the 2-iminopyridine moiety.

A few years ago, we studied the stereochemistry of 3-isocyanatoacrylonitrile.[35] In these isocyanates, the *N*-inversion provides a mechanism to interconvert C−N conformers of *E*- or *Z*-configured alkenes and we found these isomerizations to proceed via nonplanar transition state structures. The practical relevance of this finding is limited because of the very low activation barriers ($\Delta E_A \ll RT$). In contrast, the results discussed here show that the activation barriers to *N*-inversion of the heteroarene imines are about 20 kcal/mol and, hence, it should be possible to measure their isomerization kinetics by variable-temperature NMR spectroscopy.

The most direct experimental approach would involve stereospecific synthesis of the (*Z*)-imine and the study of its reaction to the amino-tautomer, i.e., (*Z*)-**PMI** → (*E*)-**PMI** → **APM**. In a more practical and more promising approach, one would prevent the asymmetric amidine−amidine tautomerization that converts the exocyclic imine to an amino group (i.e., (*E*)-**PMI** → **APM**) and study the (*E*)/(*Z*)-isomerization of the respective *N*-alkyl derivatives. For example, 3-methylpyrimidin-4(3*H*)-imine (**3MePMI**), 1-methylpyridin-2(1*H*)-imine[36] (**1MePYI**), and 1-methyl-1*H*-purine-6(9*H*)-imine[37] (**1MePUI**) all are synthetically accessible.

Acknowledgment. We thank Drs. Gordon Springer and Larry Sanders for their assistance with computational hardware and software. Dr. Stephen Montgomery-Smith suggested a suitable function for the generation of the potential energy surface shown in Scheme 3. MU Research Computing is supported by Federal Earmark NASA Funds for Bioinformatics Consortium Equipment and additional support from Dell, SGI, Sun Microsystems, TimeLogic, and Intel.

Supporting Information Available: Cartesian coordinates of stationary structures of **PMI**, **PYI**, and **PUI** computed at MP2/6-31G(d), CCSD/6-31G(d), and CCSD/6-31+G(d). This material is available free of charge via the Internet at http://pubs.acs.org.

(35) Glaser, R.; Wu, H.; Saint-Paul, F. v. Chemical carcinogens in non-enzymatic cytosine deamination: 3-isocyanatoacrylonitrile. In *J. Mol. Model.* **2006**, *12*, 731–737.

(36) Buurman, D. J.; van der Plas, H. C. Imination of *N*-Methylpyridinium Salts by Liquid Ammonia-Potassium Permanganate [1]. A New Synthesis of Nudiflorine. In *J. Heterocycl. Chem.* **1986**, *23*, 1015–1018.

(37) Fujii, T.; Itaya, T. Systematic Tables of Mono- and Poly-N-Methylated Adenines: Acid Dissociation Constants and NMR Spectral Data. In *Heterocycles* **1999**, *51*, 2255–2277.